Semiclassical Theory of Quantum Chaotic Transport: Phase-Space Splitting

Ph. Jacquod[1,2] and Robert S. Whitney[1]
[1] *Département de Physique Théorique, Université de Genève, CH-1211 Genève 4, Switzerland*
[2] *Department of Physics, University of Arizona, 1118 E. Fourth Street, Tucson, AZ 85721*

We investigate transport properties of quantized chaotic systems in the short wavelength limit. We focus on non-coherent quantities such as the Drude conductance, its sample-to-sample fluctuations, shot-noise and the transmission spectrum, and we show how these transport properties are influenced by the emergence of the Ehrenfest time scale $\tau_{\rm E}$. Expressed in an optimal phase-space basis, the scattering matrix acquires a block-diagonal form as $\tau_{\rm E}$ increases, reflecting the splitting of the system into two cavities in parallel, a classical deterministic cavity (with all transmission eigenvalues either 0 or 1) and a quantum mechanical stochastic cavity. This results, among other effects, in the suppression of the Fano factor for shot-noise and the deviation of sample-to-sample conductance fluctuations from their universal value.

PACS numbers: 73.23.-b, 74.40.+k, 05.45.Mt, 05.45.Pq

I. INTRODUCTION

Closed chaotic systems are classically characterized by ergodicity, mixing and a positive Kolmogorov-Sinai (KS) entropy [1]. These three characteristics form a hierarchy: mixing systems are ergodic, and systems with positive KS entropy are mixing, but the reverse is not necessarily true. Ergodicity means that phase-space averages equal time averages, while the definition of both mixing and KS entropy requires the introduction of some phase-space coarse-graining. For mixing, one needs to define finite-sized phase-space cells inside which points originating from two initially well separated distributions of initial conditions are equally likely to be found. As time goes by, mixing occurs on smaller and smaller scales, i.e. the minimal volume of these cells decreases. The KS entropy is defined from the measure of the intersection of the cells with their back evolution under the system dynamics. A positive KS entropy means an exponential production of information, and thus the generation of randomness in the Kolmogorov sense, as more and more different trajectories emerge from apparently indistinguishable initial conditions [1]. For closed systems, the KS entropy is related to the exponential sensitivity to initial conditions, and equals the sum of the associated positive Lyapunov exponents [1, 2].

The situation becomes different once the system is open and scattering trajectories are considered. Phase-space structures emerge then which are prohibited by ergodicity and mixing, even in systems which have a positive KS entropy when closed. These structures and their influence on quantum transport are the focus of this article. We will see how their occurrence affects transport through open quantized chaotic systems in the semiclassical, short wavelength limit. They result in a splitting of the cavity into two cavities in parallel, one where transport is ruled by classical determinism and one where transport exhibits quantum stochasticity.

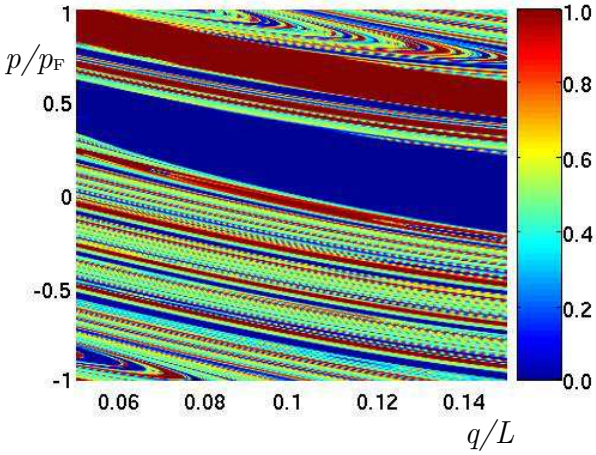

FIG. 1: (Color online) Classical phase-space color plot of the transmission probability from the phase-space projection of the injection lead (see Fig. 2). The phase-space has been coarse-grained by a rectangular grid with $9{\cdot}10^4$ nodes, and the transmission probability in each cell has been calculated by time-evolving 10^4 classical trajectories per cell. Higher transmissions correspond to red, lower transmissions to blue. The dynamical system used is the open kicked rotator as defined in Ref. [5].

A. Classical chaos in open systems

We specialize to two-dimensional chaotic cavities in a two-terminal geometry. Typical nonergodic structures occurring in such open chaotic systems are illustrated in Fig. 1. A color plot of the transmission probability is shown on a phase-space projection of one of the two openings. The horizontal axis gives the position on a cross-section of the opening, normalized by the cavity perimeter L, and the vertical axis gives the momentum component of injection into the system, parallel to the cavity boundary, and normalized by the Fermi momentum $p_{\rm F}$. Both the real-space set-up and the dimensionless

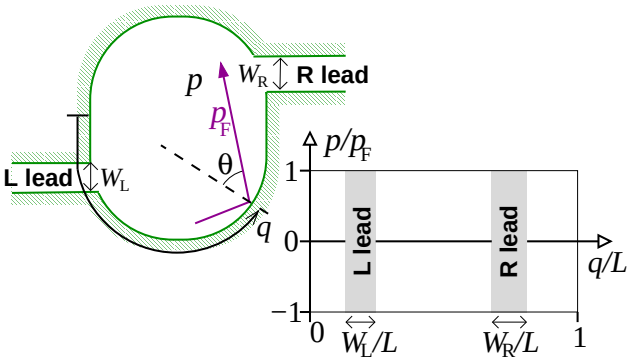

FIG. 2: (Color online) Sketch of a two-terminal open chaotic cavity (top left) and its phase-space represented as a Poincaré surface of section on the boundary of the cavity (bottom right). All momenta on the energy surface ($E = p_F^2/2m$) are parameterized by the tangential momentum p running from $-p_F$ to p_F. All possible positions on the boundary are parameterized by q running from zero to L, where L is the circumference of the cavity. The phase-space is made dimensionless by normalizing momenta and real-space coordinates with p_F and L respectively.

phase-space we use are defined in Fig. 2.

Band-like structures such as those appearing in Fig. 1 have been reported and discussed earlier [3, 4, 5, 6, 7, 8]. All scattering trajectories whose initial point lies in one of the bands have approximately the same dwell time through the system [9]. The typical dwell time τ of a band determines its width as $\simeq (W/L)\exp[-\lambda\tau]$ [4] (W is the width of the opening and λ is the Lyapunov exponent). Thus the largest blue and red bands in Fig. 1 respectively correspond to direct reflection and transmission, while thinner bands correspond to longer dwell times through the system. Trajectories inside a band are transported in one bunch, and the phase-space volume they occupy is blocked for other trajectories by Liouville's theorem. Because trajectories remain inside the system for a finite time, the definition of ergodicity, that

$$\int_\Omega \mathrm{d}\mathbf{p}\mathrm{d}\mathbf{q}\; f(\mathbf{p},\mathbf{q};t) = \lim_{\tau\to\infty} \tau^{-1} \int_0^\tau \mathrm{d}t f(\mathbf{p}_0,\mathbf{q}_0;t), \quad (1)$$

for almost all functions $f(\mathbf{p},\mathbf{q};t)$ and almost all phase space points $(\mathbf{p}_0,\mathbf{q}_0) \in \Omega$ no longer holds, but depends on $(\mathbf{p}_0,\mathbf{q}_0)$. The time-integral on the right-hand side of Eq. (1) extends only up to the dwell time t_0 of the one trajectory going through $(\mathbf{p}_0,\mathbf{q}_0)$, and accordingly Eq. (1) cannot be preserved over the full phase-space Ω. Simultaneously, mixing occurs on a given scale only for the subset of trajectories longer than some finite dwell time. Scattering trajectories through open systems have a continuous distribution of dwell times $P(t)$ and because of the exponentially decreasing volume of scattering bands, mixing occurs on exponentially smaller scales on longer trajectories. Reversing the argument, a given phase-space resolution volume ξ corresponds to a time scale $\tau_\xi \approx \lambda^{-1}\ln[(W/L)^2/\xi]$. Long trajectories with $\tau > \tau_\xi$ exhibit mixing on the scale ξ, while short trajectories with $\tau < \tau_\xi$ lie on bands well resolved by ξ-cells, which therefore do not have the mixing property. These two sets of classical scattering trajectories have no phase-space overlap.

B. Quantum chaos in open systems

A finite resolution scale emerges naturally when the system is quantized: the phase-space becomes tiled with cells of volume $2\pi\hbar$. For particles with a finite Fermi wavelength λ_F, this is equivalent to tiling the dimensionless phase-space projection of the leads (see Fig. 2) with cells of volume $\hbar_{\mathrm{eff}} = \lambda_F/L$, the effective Planck's constant. This leads to the existence of a finite number $N = \mathrm{Int}[2W/\lambda_F]$ of conduction channels through the system. As $\hbar_{\mathrm{eff}}$ is made smaller and smaller, all classical parameters being kept constant (the semiclassical limit), more and more of the band structures of Fig. 1 are resolved (see Fig. 3). Conversely, more and more of the conduction channels are supported by one and only one classical transmission or reflection band, and thereby become deterministic. It is thus natural to investigate the effect that the lack of mixing of short trajectories has on properties of open quantum chaotic systems.

Transport through ballistic quantum cavities, so-called quantum dots, has been investigated intensively in recent years [10]. In the regime where the dot's size is much larger than the Fermi wavelength, $L \gg \lambda_F$, transport has been shown to depend on the integrability or lack thereof of the classical dynamics, as determined by the confinement potential [11, 12]. Most experimental investigations so far have focused on the limit of few, $\lesssim 10$, conduction channels, where it has been found that quantum transport in the chaotic case exhibits a universality which is well captured by the Random Matrix Theory (RMT) of transport [13, 14]. Unlike for disordered metallic systems [15], there is at present no microscopic foundation for the RMT of transport in ballistic cavities, though there is little doubt that RMT applies to a broad range of such systems. We note with great interest the important steps made recently towards a proof that closed chaotic systems obey RMT [16, 17], and hope that they will be extended to open systems.

It is however well-known that physically relevant time scales restrict the range of validity of RMT. In recent years it has become clear that the *Ehrenfest* time τ_E does this in ballistic quantum chaotic systems, with RMT ceasing to be valid when τ_E becomes relevant. The Ehrenfest time is the time it takes for the chaotic classical dynamics to stretch a narrow wave packet, of spatial extension λ_F, to some relevant classical length scale $\mathcal{L}$. Since the stretching is exponential in a chaotic system, one has $\tau_E = \lambda^{-1}\ln[\mathcal{L}/\hbar_{\mathrm{eff}}L]$ [18]. The scattering of an initially localized wavepacket into all possible modes (similar to s-wave scattering on a restricted portion of

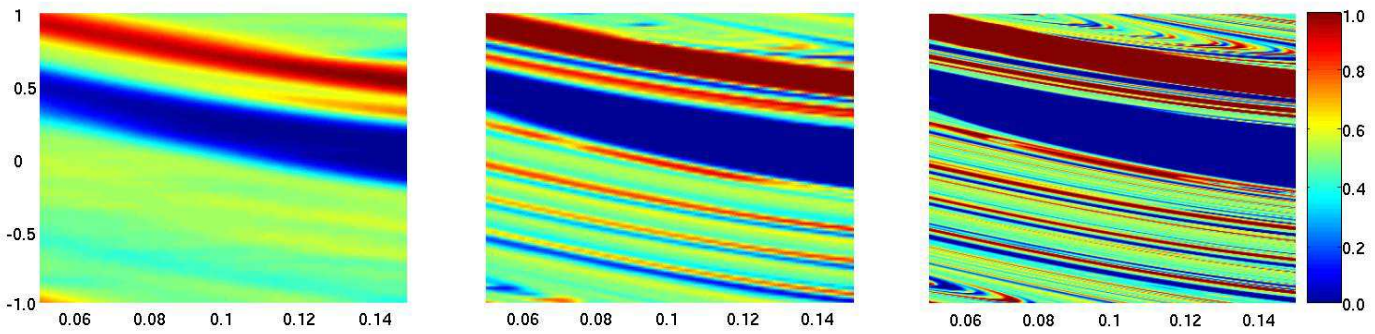

FIG. 3: (Color online) Quantum phase-space color plots of the transmission probability from the injection lead. The system is the quantum equivalent of the classical system of Fig. 1. The phase-space has been coarse-grained by a rectangular grid with $9 \cdot 10^4$ points. Starting from each point of the grid, an isotropic Gaussian wave-packet has been time-evolved and its transmission probability calculated. From left to right, the three panels correspond to decreasing effective Planck's constant $\hbar_{\rm eff} = 2\pi/M$ with $M = 512$ (with a conductance $g = 22.4$ and a Fano factor $F = 0.193$), 8192 ($g = 375.9$ and $F = 0.121$) and 131072 ($g = 5990.8$ and $F \approx 0.08$) respectively. More and more fine-structured details of the classical phase-space are resolved as $\hbar_{\rm eff} \to 0$. Higher transmissions correspond to red, lower transmissions to blue color.

phase-space) is only established after classical mixing has set in on the scale $\hbar_{\rm eff}$, i.e. for times longer than $\tau_{\rm E}$. For shorter times, the quantum dynamics is deterministic. One thus expects deviations from RMT to emerge as $\tau_{\rm E}/\tau_{\rm D}$ increases.

This line of reasoning has been qualitatively confirmed in the cavity transport experiments of Ref. [19], which observed a significant reduction of the electronic shot-noise power below its RMT value upon opening the cavity more and more. This reduction is very likely due to an increasing fraction of deterministic channels in the transmission spectrum of the cavity which can be understood as follows. The shot-noise power (the zero-temperature zero-frequency current-current correlator) is usually quantified by the dimensionless Fano factor F, the ratio of the shot-noise to the Poissonian noise [20], which can be expressed in term of the transmission spectrum $T_i \in [0, 1]$ of the cavity as [20]

$$F = \sum_i T_i(1 - T_i) \Big/ \sum_i T_i. \qquad (2)$$

Hence deterministic channels, those having $T_i = 0$ or 1, do not contribute to F. Such channels appear as the classical bands discussed above are quantum mechanically resolved, which can be achieved either by reducing the dwell time or by reducing the Fermi wavelength. The former change was more appropriate for the experimental set-up of Ref. [19], and the latter change is illustrated in the numerics of Fig. 3. We show three quantum phase-space plots for a fixed classical set-up (the same as for Fig. 1). Plotted is the quantum transmission probability $\langle (x,p)|\mathbf{T}|(x,p)\rangle$ for a fixed grid of initial coherent states $|(x,p)\rangle$, i.e. isotropic Gaussian wavepackets centered on (x,p). The three panels from left to right correspond to smaller and smaller $\lambda_{\rm F}$. It is seen that as $\lambda_{\rm F}$ decreases, finer and finer phase-space structures are resolved. Moreover, coherent states entirely lying on deep red (deep blue) regions have $\langle (x,p)|\mathbf{T}|(x,p)\rangle = 1$ (0), and are therefore eigenstates of $\mathbf{T}$. Any of them can carry a quantum channel which does not contribute to shot-noise (the total number of deterministic channels is obtained only after the orthogonalization of the coherent states, see below). With decreasing $\lambda_{\rm F}$, the number of deterministically transmitted coherent states increases faster than the total number of channels, reducing the shot-noise power below its RMT value.

The suppression of the Fano factor in the semiclassical limit was anticipated long ago [21]. More recent works quantitatively predicted a suppression $F \propto \exp(-\tau_{\rm E}/\tau_{\rm D})$, in term of the new Ehrenfest time scale and the average dwell time $\tau_{\rm D}$ through the system [22], a suppression which was related to the phase-space resolution picture of Ref. [4] given above and confirmed numerically in Refs. [5, 7]. Ref. [23] presented a phase-space semiclassical approach resolving the classical bands which showed that the fraction of deterministic transmission eigenvalues not contributing to noise is $\propto [1 - \exp(-\tau_{\rm E}/\tau_{\rm D})]$. Following the numerous recent investigations of the quantum-to-classical correspondence in open systems, which we now proceed to briefly summarize, it has become clear that $\tau_{\rm E}/\tau_{\rm D} \to 0$ is a necessary condition for complete RMT universality [24]. As is illustrated in Fig. 4, this condition is never satisfied in the semiclassical limit $\hbar_{\rm eff} \to 0$.

Following Ref. [25] which suggested that the existence of a finite $\tau_{\rm E}$ discriminates quantum chaotic from quantum disordered systems (with the former class exhibiting deviations from universality), many investigations have been devoted to the study of open quantum chaotic systems at finite $\tau_{\rm E}$ [24]. Focusing on transport, it is by now well established numerically that, as $\tau_{\rm E}/\tau_{\rm D} \to \infty$, the Fano factor disappears [5], and sample-to-sample con-

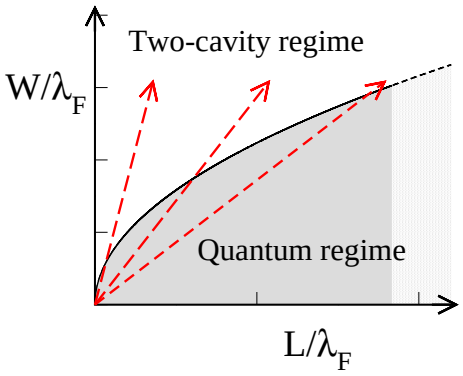

FIG. 4: (Color online) Schematic of the different transport regimes through a ballistic chaotic cavity with perimeter L coupled to leads of width W. Above the separatrix $W = (\lambda_F L)^{1/2}$ (solid curve), we have $\tau_E > 0$ (see Eq. 8) and the system splits into two effective cavities, one classical and the other quantum. Only the latter contains quantum effects such as non-deterministic transmission and quantum interferences. Below the separatrix $\tau_E = 0$ and all modes are quantum (grey area). The red dashed arrows indicate the semiclassical limit of $\hbar_{\rm eff} \to 0$ at fixed classical parameters. The slope of the arrows is given by the inverse dwell time τ_D.

ductance fluctuations lose their universality, while simultaneously, parametric conductance fluctuations remain universal [6, 7]. The fate of weak localization is, as of yet, unclear. The predictions of Refs. [25, 26] that weak localization corrections also disappear exponentially with τ_E/τ_D have been first challenged [27], but later supported [28].

There are currently several theories for open quantum chaotic systems at finite τ_E. First, the stochastic quasiclassical theory mimics the post-Ehrenfest time mode-mixing by introducing fictitious random scatterers with a scattering rate appropriately tuned [25, 28]. It is developed from standard methods in disordered systems, but breaks time-reversal symmetry at the classical level [28]. Second, there is a semiclassical theory, which in its current stage violates the unitarity of the scattering matrix [26, 29]. Third, a phenomenological model originating from Ref. [4] models the total electronic fluid as two coexisting phases, a classical and a quantum one. At this level, the theory is referred to as the two-phase fluid model [7, 23]. With the additional conjecture made in Ref. [4] that the quantum phase has RMT properties, one gets the effective RMT model. The effective RMT model successfully explains the behavior of shot-noise, the transmission spectrum and conductance fluctuations, but is in contradiction with the recently reported disappearance $\propto \exp(-\tau_E/\tau_D)$ of weak localization [28]. The exponential disappearance of weak localization, if confirmed, would invalidate the effective RMT model, but not the two-phase fluid model. The suppression of weak localization is at present unreconcilable theoretically with the survival of parametric conductance fluctuations at their universal value [6, 7].

C. Outline of this article

In this article, we focus on non-coherent quantities such as the average conductance, shot-noise and the transmission spectrum in ballistic chaotic cavities as $\hbar_{\rm eff} \to 0$. These transport properties are strongly influenced by the emergence of the open cavity Ehrenfest time, which for a symmetric configuration reads $\tau_E = \lambda^{-1} \ln[(W/L)^2/2\pi\hbar_{\rm eff}]$ [30]. All classical parameters being fixed, that limit inevitably turns any system into a nonuniversal quantum chaotic one as τ_E increases (see Fig. 4). We calculate the scattering matrix in a basis that optimally resolves phase-space structures and show that the system splits into two cavities in parallel. This provides a foundation for the two-phase fluid model. We go significantly beyond Ref. [23], with an explicit and detailed construction of a basis which optimally resolves those phase-space structures. We avoid the controversy related to coherent effects, which will be discussed in a follow-up article.

The outline of the paper goes as follows. In Section II, we discuss the nonergodic classical structures of open chaotic systems such as those shown in Fig. 1 and the Ehrenfest time scale that accompanies them. Our task requires that we resolve quantum-mechanically these classical phase-space structures. This suggests that we employ a semiclassical theory. The existing such theories [11, 31] have to be replaced by a phase-space resolving theory, which requires the construction of an appropriate orthogonal mode basis. This is done is Section III. We then write the system's scattering matrix in this basis, and show how this results in phase-space splitting at the quantum level in Section IV. Amplifying on that, we show how deterministic modes emerge and calculate the average Drude conductance and its sample-to-sample fluctuations at large τ_E. Summary and conclusions are presented in Section V, and technical details discussed in the Appendices.

II. CLASSICAL SCATTERING STRUCTURES AND EHRENFEST TIMES

A. Transmission and reflection bands

We consider classical scattering trajectories. They are injected into the cavity from one of the two leads, say the left (L) lead, with initial position q and momentum p on a cross-section of the lead. The momentum is on the Fermi energy surface $E = p_F^2/2m$. The trajectory is determined by ballistic motion inside the confinement potential defining the cavity, until the particle hits the boundary between the cavity and one of the leads, at what time it escapes. Throughout this paper we will consider perfectly transparent leads.

Scattering trajectories are not isolated, instead they occur in bands (see Fig. 1). As mentioned in the introduction, a scattering band is a phase-space structure

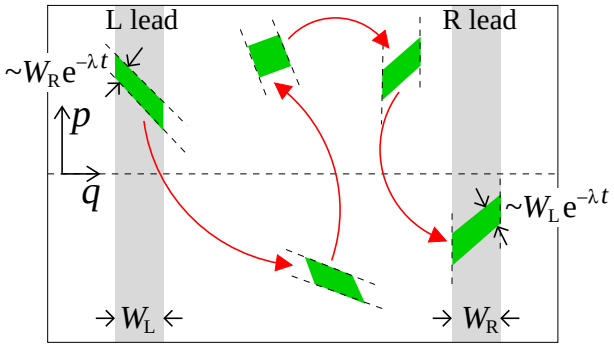

FIG. 5: (Color online) Time evolution of an L to R transmission band (parallelograms) on the boundary of the cavity of Fig. 2. The leads are indicated by the shaded rectangles.

occurring in open systems, even when their closed counterpart is fully chaotic. It contains a set of trajectories which exit at approximately the same time through the same lead [9], having followed similar paths through the cavity, in the sense that any trajectory in the band can be topologically deformed into any other. The situation is sketched in Fig. 5. Bands on the injection lead are defined by the overlap of that lead with the time-reversed evolution of the exit lead, including absorption at both leads.

For an individual system, the exact number and area of the bands depends on the specifics of the lead positions and widths, and the cavity shape. However, averaged properties calculated over an ensemble of cavities with the same dwell time and Lyapunov exponent can be calculated. The asymptotic average survival probability is exponential [32],

$$\rho(\tau) = \exp[-\tau/\tau_{\rm D}]. \tag{3}$$

It depends solely on the average dwell time $\tau_{\rm D}$ given by

$$\tau_{\rm D} = \frac{\pi A}{v_F(W_{\rm L}+W_{\rm R})}. \tag{4}$$

Here A is the area of the cavity and we considered leads with different widths $W_{L,R}$.

In the dimensionless phase-space defined in Fig. 2, where momenta and distances are measured in units of $p_{\rm F}$ and L respectively, the injection lead (we always assume this is the L lead) has a dimensionless phase space area of

$$\Sigma_{\rm L} = 2W_{\rm L}/L. \tag{5}$$

The fraction of the lead phase space which couples to transmitting trajectories is $\sim W_{\rm R}/(W_{\rm L}+W_{\rm R})$, with the rest coupling to reflecting trajectories. The average phase-space area of a single transmission (L→R) or reflection (L→L) band which exits at time τ, is given by

$$\langle \Sigma_{{\rm L}\to K}(\tau)\rangle \;\sim\; \frac{W_{\rm L}W_K}{L^2}{\rm e}^{-\lambda\tau}, \tag{6}$$

where $K = {\rm L},{\rm R}$. The average number $\langle n_{{\rm L}\to K}(\tau)\rangle$ of bands exiting at time τ through lead K is given by multiplying $\Sigma_{\rm L}/\langle\Sigma_{{\rm L}\to K}(\tau)\rangle$ by the probability $(W_K/L)\exp[-\tau/\tau_{\rm D}]$ to escape through the K lead at τ. Hence one has

$$\langle n_{{\rm L}\to{\rm L}}(\tau)\rangle = \langle n_{{\rm L}\to{\rm R}}(\tau)\rangle \;\sim\; \exp[\lambda\tau(1-(\lambda\tau_{\rm D})^{-1})]. \tag{7}$$

Since we assume fully developed chaos, $\lambda\tau_{\rm D}\gg 1$, we see that the average number of bands diverges as τ goes to infinity even though the sum of their phase-space areas goes to zero. We also note that the average number of reflection and transmission bands are equal, with only their areas being dependent on $W_{\rm L,R}$.

B. Ehrenfest times and modes on classical bands

The Ehrenfest time scale emerges out of the quantum mechanical coarse-graining of phase-space and the partial resolution of scattering bands. It is the time it takes for quantum mechanical uncertainties to blow up to some relevant classical scale $\mathcal{L}$ in chaotic systems. The scale $\mathcal{L}$ depends on the problem at hand, e.g. on whether the system is closed [18], or open [30, 33]. For the transport set-up we will focus on, this scale is related to the area of scattering bands. Large scattering bands, those with phase-space area greater than $2\pi\hbar$, can carry a number of modes of order their phase-space area divided by $2\pi\hbar$. All those modes are classical, deterministic and exhibit no quantum effects. They are supported by trajectories shorter than the Ehrenfest time. The small bands on the other hand, those with area less than $2\pi\hbar$ carry less than a full mode, which generates quantum (stochastic) modes, sitting on many small bands with dwell times longer than the Ehrenfest time, and hence being partially transmitted, partially reflected. Eq. (6) then defines two open cavity Ehrenfest times for states injected from the L lead, one for transmitting bands and one for reflecting bands

$$\tau_{\rm E}^{{\rm L}K} \;=\; \lambda^{-1}\ln\left[\frac{W_{\rm L}W_K}{2\pi\hbar_{\rm eff}L^2}\right] \quad ; \quad K={\rm L},{\rm R}. \tag{8}$$

The difference between $\tau_{\rm E}^{\rm LR}$ and $\tau_{\rm E}^{\rm LL}$ is only logarithmic in $W_{\rm R}/W_{\rm L}$. We will often neglect it and consider instead the symmetric open cavity Ehrenfest time $\tau_{\rm E} = \lambda^{-1}\ln[(W/L)^2/2\pi\hbar_{\rm eff}]$. The open cavity Ehrenfest times, $\tau_{\rm E}^{{\rm L}K}$ can be interpreted as the time it takes for a wavepacket of width $W_{\rm L}/L$ along the stable manifold of the hyperbolic classical dynamics to evolve into a wavepacket with width W_K/L in the unstable direction.

We can readily estimate the number of quantum scattering modes. The proportion of the L lead phase space which couples to trajectories to the K lead with $\tau > \tau_{\rm E}^{{\rm L}K}$ is on average ${\rm e}^{-\tau_{\rm E}^{{\rm L}K}/\tau_{\rm D}}W_K/(W_{\rm L}+W_{\rm R})$. Thus the average number of quantum modes in the L lead is

$$\langle N_{\rm L}^{\rm qm}\rangle \;=\; N_{\rm L}\frac{N_{\rm L}{\rm e}^{-\tau_{\rm E}^{\rm LL}/\tau_{\rm D}}+N_{\rm R}{\rm e}^{-\tau_{\rm E}^{\rm LR}/\tau_{\rm D}}}{N_{\rm L}+N_{\rm R}}. \tag{9}$$

All other modes of the L lead are in transmission bands with $\tau < \tau_{\rm E}^{\rm LR}$ or reflection bands with $\tau < \tau_{\rm E}^{\rm LL}$, and so they are all classical modes. Their number is thus

$$\begin{aligned}\langle N_{\rm L}^{\rm cl}\rangle &= N_{\rm L} - \langle N_{\rm L}^{\rm qm}\rangle \\ &= N_{\rm L}(1-{\rm e}^{-\tau_{\rm E}^{\rm LR}/\tau_{\rm D}}) + \mathcal{O}[(\lambda\tau_{\rm D})^{-1}]. \end{aligned} \quad (10)$$

The counting argument leading to these estimates finds a rigorous derivation below in section III B, where we explicitly cover scattering bands with an orthonormal phase-space (PS) basis. There, we also identify a third class of states, overlapping significantly but still only partially with large bands with $\tau < \tau_{\rm E}^{LK}$. Because of their small relative number however, these states only have a subdominant effect on the system's properties.

Note that the number of classical PS-states goes like $\hbar_{\rm eff}^{-1}(1-\hbar_{\rm eff}^{-1/(\lambda\tau_{\rm D})})$, while the number of quantum PS-states goes like $\hbar_{\rm eff}^{-1-1/(\lambda\tau_{\rm D})}$. In the semiclassical limit $\hbar_{\rm eff}\to 0$ we see that the number of quantum PS-states goes to infinity, while their fraction goes to zero.

III. THE PHASE-SPACE BASIS

In order to formally split classical from quantum modes, our task now is to construct a complete orthonormal basis resolving maximally the scattering band structure of the classical phase-space. This requires an optimal resolution in both real-space and momentum coordinates. To achieve that, we use results from wavelet analysis.

A. Existence of orthogonal phase-space bases

The existence of complete orthonormal bases with states exponentially localized in time and frequency has been proven in the context of wavelet analysis [34]. We use such a basis as a PS-basis, in which each basis state is exponentially localized in position and momentum. We are unaware of any such basis which has closed form expressions for the basis states. There are however numerous algorithms for generating such bases [34]. In Appendix B we give such an algorithm which iteratively orthogonalizes a complete but non-orthogonal basis of coherent states, generating a set of PS-states of the form shown in Fig. 6. While we give this explicit example, we emphasize that our theory only requires the existence of such a basis. We use the fact that each basis state is exponentially localized in position and momentum, and that any such complete orthonormal basis remains complete and orthonormal under any rotation, translation or area-preserving stretch in phase-space. Having constructed the PS-basis, the transformation which takes us from lead modes to PS-states is unitary since both bases are orthonormal.

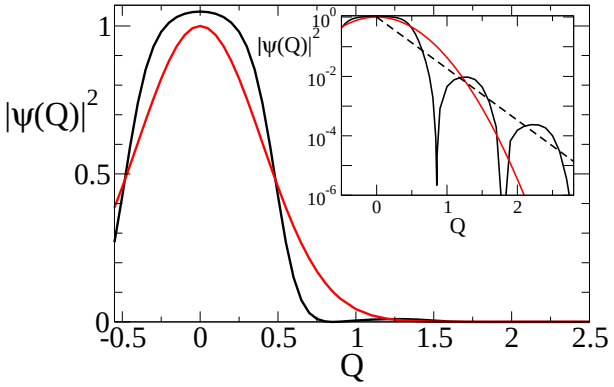

FIG. 6: (Color online) Main plot: Plot of the real-space wavefunction components $|\langle Q|{\rm ps};0,0\rangle|^2$ of a PS-basis state (black line), and $|\langle Q|{\rm cs};0,0\rangle|^2$ of a coherent state (red line). Both wavefunctions are symmetric in the dimensionless phase-space under $Q\leftrightarrow P$, up to a scaling factor. Inset: Logarithmic plot of $|\langle Q|{\rm ps};0,0\rangle|^2$, showing that the PS-state decays exponentially in position (dashed line). The oscillations in $|\langle Q|{\rm ps};0,0\rangle|^2$ ensures it is orthogonal to PS-states centered at finite Q, while its broader central peak ensures that it is orthogonal to PS-states centered at finite P.

B. The optimal phase-space basis

In a recent letter [23], we constructed an orthonormal PS-basis on a square von Neumann lattice. This basis is simple to explain and work with, however, it underestimates the number of classical modes and in particular leads one to predict that the open cavity Ehrenfest time is half its correct value [35]. To obtain the correct value of $\tau_{\rm E}$, the von Neumann lattice must be adapted to fit in the classical band structures as best as it can. This is done band by band. For parallelogram bands, the procedure is to rotate and stretch the originally square von Neumann lattice to a parallelogram von Neumann lattice. This is illustrated in Fig. 7. Each lattice cell still covers an area $2\pi\hbar$ and the intraband orthogonality is ensured. The interband basis orthogonality is preserved due to the exponentially small overlap of PS-basis states in different bands (classical bands do not overlap thanks to Liouville's theorem), except for a minority of states lying directly at the boundary of the band which we will deal with below. This procedure can still be applied as long as the band's curvature is not too large, or for bands which look more trapezoidal than parallelogram-like. All one needs to do then is adapt locally the aspect ratio of the von Neumann lattice, as shown on Fig. 8. Bands with small curvatures dominate at short dwell times. However, some bands with larger dwell times inevitably display a fold. For those bands, the procedure is to bend the von Neumann lattice along the axes defined by the eigenvectors of the stability matrix of the classical dynamics at each point in the band's phase space, as in Fig. 8. The aspect ratio of the lattice is chosen so it obeys Eq. (11) locally. For intermediate values of $\hbar_{\rm eff}$,

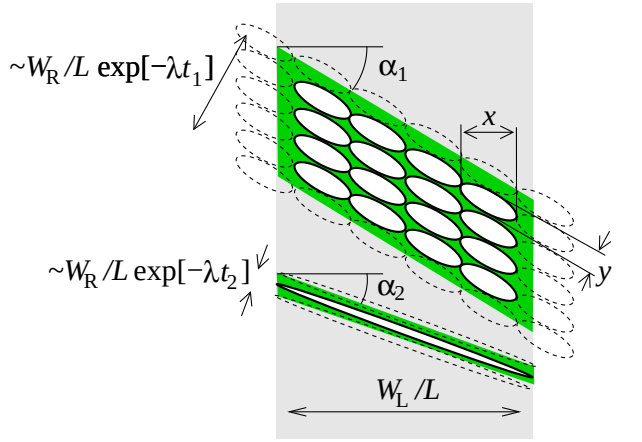

FIG. 7: (Color online) Sketch of two parallelogram bands (green areas) with the PS-states superimposed on them (ellipses). The upper band has a phase-space area which is a bit more than sixteen times $2\pi\hbar$, while the lower band has a phase-space area a bit more than $2\pi\hbar$. In both cases the basis is optimized, the lattice of PS-states is stretched and rotated such that the maximum number of PS-states can be fitted into each band (solid-edged ellipses) with the minimum number partially in the band (dashed-edged ellipses). Note that these optimally chosen PS-states have the same aspect ratio as the classical band in which they sit, thus their longitudinal and transversal extensions, x and y, are given by Eq. (11).

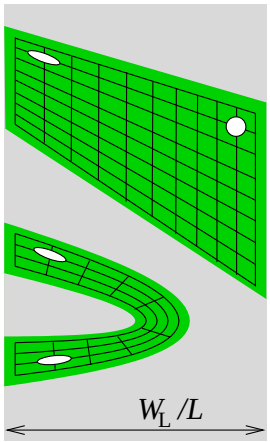

FIG. 8: (Color online) Sketch of a trapezoidal (top green area) and a folded (bottom green area) scattering band with a lattice of PS-states superimposed on them. Both bands cover a phase-space area larger than $2\pi\hbar$. In both cases the basis is optimized, the lattice of PS-states is locally stretched and rotated such that the maximum number of PS-states can be fitted into each band, some of them are indicated by solid-edged ellipses.

the local curvature of the resulting lattice destroys the orthogonality of the PS-states, however, as $\hbar_{\rm eff}$ is reduced further and further, the curvature drops out of the problem, any smooth curve being locally well approximated by a straight line. To formally show that an optimal orthogonal basis can be generated from the square von Neumann basis of Ref. [23] it is thus sufficient to (i) consider parallelogram and trapezoidal bands only, keeping in mind however that (ii) at any finite value of $\hbar_{\rm eff}$, deviations from parallelogram shape generates additional non-optimal PS-basis states. The latter result from a further orthogonalization (e.g. Gram-Schmidt) required for edge-of-band states and for states on folds whose curvature is not yet well resolved at this value of $\hbar_{\rm eff}$. Below in Appendix C we will see that those states build up a negligible fraction $N_{\rm qm}/(\lambda\tau_{\rm D}) \ll N_{\rm qm} \ll N_{\rm cl}$ of the total number of modes in the semiclassical limit. The completeness of the basis follows from the orthogonality and the conservation of the total number of basis states, the above procedure being area-conserving. We are now ready to extend the discussion of Ref. [23] and derive an optimal phase-space basis for parallelogram bands, which gives the correct Ehrenfest time. This is done in a four step process.

Step [i]. Pick a scattering band with phase-space area larger than $2\pi\hbar$, and cover it with a lattice of PS-states. Both the lattice and the states must be stretched and rotated to the same angle and aspect ratio as the band, and positioned in such a way as to minimize the number of edge-of-band states. This is illustrated in Fig. 7. This can be done without relaxing either the mutual orthogonality, or the normalization of the PS-states. Since the PS-states have the same aspect ratio as the band, their longitudinal and transversal extensions x and y, as indicated in Fig. 7, are given by (τ is the dwell time of the band under consideration)[36]

$$x \simeq (2\pi\hbar_{\rm eff} W_{\rm L}/W_{\rm R})^{1/2} \exp[\lambda\tau/2] \;\; ; \;\; y \simeq 2\pi\hbar_{\rm eff}/x. \quad (11)$$

While we pay attention to minimizing their number, we do not include edge-of-band states in the basis at this stage. We will deal with them later in step [iv].

Step [ii]. We evolve the states generated in step [i] under the cavity's dynamics. The lattice of PS-states on an injection band uniquely determines the lattice of PS-states on the exit band. All trajectories in the band under consideration exit the cavity after a time shorter than the open cavity Ehrenfest time. On this time scale the quantum dynamics of the PS-states are well approximated by the Liouville flow [37] (see also Appendix A). This is a well-known property of coherent states that can be extended to the exponentially localized PS-states that we consider here. Thus a PS-state with initial spread of ΔQ in the unstable direction at $\tau = 0$, will evolve into a PS-state with spread $\Delta Q' \sim \Delta Q e^{\lambda\tau}$ in the unstable direction at time τ. The initial spread in the stable direction is $\Delta P \simeq \hbar/\Delta Q$, and since the quantum dynamics is Liouvillian inside classical bands, it is area preserving, i.e. $\Delta P' \simeq \hbar/\Delta Q'$. The PS-states are stretched and rotated in the same manner as the exiting band, while still forming an orthonormal basis on that band. The orientation and stretch of the lattice and PS-states are given in linear approximation (which eventually become valid as $\hbar_{\rm eff} \to 0$) by the eigenvalues and eigenvectors of

the stability matrix of the classical dynamics, and thus have the same aspect ratio and angle as the exiting band. We choose to use these states to cover that band in the phase-space.

Step [iii]. We simply repeat the process in steps [i-ii] for each band with area $> 2\pi\hbar$ not yet covered by PS-states. The crucial point here is that bands cannot overlap; hence if we only place PS-states within classical bands, PS-states in different bands must be orthogonal with exponential accuracy.

Step [iv]. Steps [i-iii] generate an incomplete orthonormal basis in the vector-space of lead modes. This basis can be made complete by adding the adequate number of states orthogonal to those generated in steps [i-iii]. This construction gives us very little information about the nature of these additional states, except that they must sit on more than one band. They thus evolve in a quantum, stochastic manner, and we refer to them as quantum PS-states. The set of quantum PS-states divides into two broad categories: firstly those which sit on many classical bands, secondly those which sit mostly, but not completely on a single band. We already mentioned the second category of edge-of-band PS-states (the dashed ellipses in Fig. 7). In Appendix C we estimate that the number of edge-of-band PS-state is

$$N_{\rm eob} \simeq (\lambda\tau_{\rm D})^{-1} N_{\rm qm} \tag{12}$$

Hence they form a small fraction of the total number of quantum modes, and we do not consider them separately from pure quantum modes.

IV. SCATTERING MATRIX IN THE PHASE-SPACE BASIS

A. Splitting of the scattering matrix and deterministic transmission

By construction, the PS-basis is chosen so that there is a one-to-one correspondence between incoming and outgoing classical PS-states, given that their quantum dynamics can be approximated by the Liouvillian flow. The unitarity of the scattering matrix means that the quantum PS-states remain orthogonal to the classical ones as they evolve inside the cavity. Thus, despite the fact that quantum PS-states are not well described by the Liouvillian flow, they cannot penetrate the regions of phase space containing bands larger than $2\pi\hbar_{\rm eff}$. In the PS-basis, each incoming classical PS-state goes to exactly one outgoing classical PS-state, while each incoming quantum PS-state goes to multiple outgoing quantum PS-states, but no outgoing classical PS-states. Correspondingly, the scattering matrix in the PS-basis is of the form

$$\mathcal{S} = \mathcal{S}_{\rm cl} \oplus \mathcal{S}_{\rm qm} = \begin{pmatrix} \mathcal{S}_{\rm cl} & 0 \\ 0 & \mathcal{S}_{\rm qm} \end{pmatrix}. \tag{13}$$

The matrix $\mathcal{S}_{\rm cl}$ is $N^{\rm cl}\times N^{\rm cl}$ while the matrix $\mathcal{S}_{\rm qm}$ is $N^{\rm qm}\times N^{\rm qm}$, with $N^{\rm cl} = N_{\rm L}^{\rm cl} + N_{\rm R}^{\rm cl}$ and $N^{\rm qm} = N_{\rm L}^{\rm qm} + N_{\rm R}^{\rm qm}$.

The matrix $\mathcal{S}_{\rm cl}$ has only one non-zero element in each row and each column. The modes on the left and right of $\mathcal{S}$ can be reordered such that the transmission part $\mathbf{t}_{\rm cl}$ of $\mathcal{S}_{\rm cl}$ is diagonal with all its non-zero elements in the first n elements of its diagonal, where n is the number of classical transmission modes. Thus we can write

$$\mathbf{t}_{\rm cl} = \begin{pmatrix} \tilde{\mathbf{t}}_{\rm cl} & 0 \\ 0 & 0 \end{pmatrix}, \tag{14}$$

where all non zero-elements of $\mathbf{t}_{\rm cl}$ are contained in the $n\times n$ matrix $\tilde{\mathbf{t}}_{\rm cl}$. Doing the same for $\mathbf{t}'_{\rm cl}$, $\mathbf{r}_{\rm cl}$ and $\mathbf{r}'_{\rm cl}$, we write the classical part of the scattering matrix as

$$\mathcal{S}_{\rm cl} \equiv \begin{pmatrix} \mathbf{r}_{\rm cl} & \mathbf{t}'_{\rm cl} \\ \mathbf{t}_{\rm cl} & \mathbf{r}'_{\rm cl} \end{pmatrix} = \begin{pmatrix} 0 & 0 & \tilde{\mathbf{t}}'_{\rm cl} & 0 \\ 0 & \tilde{\mathbf{r}}_{\rm cl} & 0 & 0 \\ \tilde{\mathbf{t}}_{\rm cl} & 0 & 0 & 0 \\ 0 & 0 & 0 & \tilde{\mathbf{r}}'_{\rm cl} \end{pmatrix}, \tag{15}$$

where $\tilde{\mathbf{t}}_{\rm cl}$ and $\tilde{\mathbf{t}}'_{\rm cl}$ are $n\times n$ matrices, $\tilde{\mathbf{r}}_{\rm cl}$ is an $(N_L^{\rm cl} - n)\times(N_L^{\rm cl} - n)$ matrix and $\tilde{\mathbf{r}}'_{\rm cl}$ is an $(N_R^{\rm cl} - n)\times(N_R^{\rm cl} - n)$ matrix. The matrix $\tilde{\mathbf{t}}_{\rm cl}$ is diagonal with elements given by

$$(\tilde{\mathbf{t}}_{\rm cl})_{ij} = {\rm e}^{{\rm i}\Phi_i}\delta_{ij}\ . \tag{16}$$

The matrix $\tilde{\mathbf{r}}_{\rm cl}$ also has exactly one non-zero element in each row and each column. Its elements obey

$$|(\tilde{\mathbf{r}}_{\rm cl})_{ij}| = |(\tilde{\mathbf{r}}_{\rm cl})_{ji}| = \begin{cases} 1 & \text{when } i \text{ reflects to } j, \\ 0 & \text{otherwise.} \end{cases} \tag{17}$$

We next calculate the transmission matrix, $\mathbf{T} = \mathbf{t}^\dagger\mathbf{t}$. The block diagonal nature of $\mathcal{S}$ in the PS-basis given in Eq. (13), ensures that $\mathbf{T}$ has the same structure in that basis, hence

$$\mathbf{T} = \mathbf{T}_{\rm cl} \oplus \mathbf{T}_{\rm qm} = \begin{pmatrix} \mathbf{T}_{\rm cl} & 0 \\ 0 & \mathbf{T}_{\rm qm} \end{pmatrix}, \tag{18a}$$

$$\mathbf{T}_{\rm cl} = \mathbf{t}_{\rm cl}^\dagger\mathbf{t}_{\rm cl} \quad ; \quad \mathbf{T}_{\rm qm} = \mathbf{t}_{\rm qm}^\dagger\mathbf{t}_{\rm qm}\ . \tag{18b}$$

From Eq. (14,16) we get the eigenvalues of $\mathbf{T}_{\rm cl}$,

$$T_i = \begin{cases} 1 & \text{for } 1 \le i \le n, \\ 0 & \text{for } n < i \le N_{\rm L}^{\rm cl}. \end{cases} \tag{19}$$

This is what we believe is the first proof of a longstanding hypothesis, that in the classical limit the vast majority of transmission eigenvalues are zero or one [21]. We know that there are $N_{\rm L}^{\rm cl}$ such classical modes, with the remaining modes having a quantum nature, making them unlikely to have transmission eigenvalues which are exactly zero or one. The block-diagonal structure (18) of the transmission matrix means that the dimensionless conductance, $g = \sum_i T_i$ and the Fano factor for shot noise of Eq. (2), can be written as

$$g = g_{\rm cl} + g_{\rm qm}, \tag{20}$$

$$F = \frac{g_{\rm cl}F_{\rm cl} + g_{\rm qm}F_{\rm qm}}{g_{\rm cl} + g_{\rm qm}}. \tag{21}$$

where we have introduced the conductance and Fano factor for the two cavities (classic and quantum), $g_{\rm cl,qm} = \sum_{i\in{\rm cl,qm}} T_i$ and $F_{\rm cl,qm} = [\sum_{i\in{\rm cl,qm}} T_i(1-T_i)]/[\sum_{i\in{\rm cl,qm}} T_i]$. From Eq. (19) we see that

$$g_{\rm cl} = n \qquad ; \qquad F_{\rm cl} = 0. \tag{22}$$

Anticipating the calculation of the average values $\langle g_{\rm cl,qm}\rangle$ (see next subsection),

$$F = F_{\rm qm}\exp[-\tau_{\rm E}^{\rm LR}/\tau_{\rm D}]. \tag{23}$$

Since $F_{\rm qm} < 1$, one see there is an exponential suppression of F.

The PS-basis does not give us much information about the quantum PS-states. However since each incoming PS-state sits on multiple bands, exiting at different times, it must couple to multiple outgoing PS-states. It is extremely rare for these outgoing PS-states to be all transmitting (or all reflecting), and thus we expect that the vast majority of their transmission eigenvalues lie between zero and one, and thus contribute to shot-noise. The fact that quantum and classical PS-states exist in two separate sub-blocks of the scattering and transmission matrices, see Eqs. (13) and (18), establishes the two-phase fluid model [7]. However while we know that $\mathcal{S}_{\rm qm}$ carries quantum effects, we do not know if it is well-described by RMT within its sub-space, so the validity of the effective RMT model [4] remains an open question.

B. The average Drude conductance

From the estimates in Section II B, the ensemble-averaged Drude conductance is the sum of the Drude conductances of the quantum and classical cavities,

$$\langle g\rangle_{\rm D} = \langle g_{\rm qm}\rangle + \langle g_{\rm cl}\rangle, \tag{24a}$$

$$\langle g_{\rm qm}\rangle = \frac{N_{\rm L}^{\rm qm}N_{\rm R}^{\rm qm}}{N_{\rm L}^{\rm qm}+N_{\rm R}^{\rm qm}} = \frac{N_{\rm L}N_{\rm R}}{N_{\rm L}+N_{\rm R}}{\rm e}^{-\tau_{\rm E}^{\rm LR}/\tau_{\rm D}}, \tag{24b}$$

$$\langle g_{\rm cl}\rangle = \frac{N_{\rm L}^{\rm cl}N_{\rm R}^{\rm cl}}{N_{\rm L}^{\rm cl}+N_{\rm R}^{\rm cl}} = \frac{N_{\rm L}N_{\rm R}}{N_{\rm L}+N_{\rm R}}[1-{\rm e}^{-\tau_{\rm E}^{\rm LR}/\tau_{\rm D}}]. \tag{24c}$$

Thus the ensemble averaged Drude conductance is,

$$\langle g\rangle_{\rm D} = N_{\rm L}N_{\rm R}/(N_{\rm L}+N_{\rm R}). \tag{25}$$

The splitting of the cavity has little effect on $\langle g\rangle_{\rm D}$, even though classical modes and quantum modes do not mix. For strong asymmetry there is an additional term of order $N_L(\lambda\tau_{\rm D})^{-2}$ on the right of Eq. (24c), however our calculation is not valid to that order because we ignored various order $(\lambda\tau_{\rm D})^{-1}$ terms, such as edge-of-band states, in Eq. (10).

C. Sample-to-sample conductance fluctuations

Cavity splitting however strongly influences the sample-to-sample conductance fluctuations. The precise shape, size and number of the nonergodic phase-space structures fluctuates from sample to sample. These fluctuations are of a classical nature, and as such they induce the departure of conductance fluctuations from their universal behavior [6, 7]. Indeed, once $\hbar_{\rm eff}$ is small enough that quantum mechanics resolves the largest scattering band on average, the sample-to-sample conductance fluctuations are dominated by the band fluctuations. Since each resolved band carries a number $\propto \hbar_{\rm eff}^{-1}$ of channels, one expects sample-to-sample conductance fluctuations to exceed the universal value in the semiclassical limit,

$$\sigma(g) \propto \hbar_{\rm eff}^{-1} \gg 1. \tag{26}$$

The above argument predicts the onset for deviations of $\sigma(g)$ from its universal behavior once the largest band is quantum mechanically resolved, i.e. for $\hbar_{\rm eff} < (W/L)^2\exp[-\lambda\tau_0]$, where τ_0 is the minimal escape time, of order the time of flight through the cavity. Both this onset and the magnitude (26) of the sample-to-sample conductance fluctuations have been observed numerically [6, 7].

V. CONCLUSIONS

In this paper we investigated the non-coherent transport properties of open quantum chaotic systems in the semiclassical limit. We have shown how to incorporate the nonergodic structures appearing in the classical phase-space (see Fig. 1) into quantum transport. We followed the scattering approach to transport and showed how large phase-space structures result in a block-diagonal form of the scattering matrix and the splitting of the system into two sub-systems put in parallel. One of these sub-systems is of a purely classical nature, consisting of deterministic transmission modes (transmission eigenvalues are all 0 or 1). We were able to calculate the corresponding transmission eigenvalues and connect the emergence of determinism to the suppression of the Fano factor for shot-noise as well as the breakdown of universality for sample-to-sample conductance fluctuations.

At this point, the exact nature of the quantum mechanical subsystem is unknown. All its modes, however undergo a certain amount of mixing, and thus carry quantum effects. Despite many numerical results suggesting that the quantum subsystem carries RMT universality [5, 7, 8, 24, 33], this does not confirm the validity of the effective RMT model, as examples of systems exist which reproduce some, but not all, RMT features. Open regular systems with large dwell times, in particular, have a RMT transmission spectrum [38, 39], but a nonuniversal weak localization behavior [11, 40]. The recent work of

[28] implies that something similar might occur in chaotic systems for finite $\tau_{\rm E}$.

We finally point out that the phase-space method developed in this article should work as well in regular systems. We however anticipate difficulties not present in the chaotic systems treated here due to the power-law decay of the band areas and diffraction effects at the leads. The latter effects are the dominant source of stochasticity in regular systems, restoring the universality of the transmission spectrum for regular cavities with sufficiently large dwell time [38, 39].

Acknowledgments

It is a pleasure to thank İ. Adagideli and H. Schomerus for helpful discussions. This work has been supported by the Swiss National Science Foundation.

APPENDIX A: GAUSSIAN WAVEPACKETS AND HYPERBOLIC DYNAMICS

We show that the time-evolution of a Gaussian wavepacket in a uniformly hyperbolic infinite system follows the Liouvillian flow. This example supports the claim that a Gaussian wavepacket in a chaotic system follows the Liouvillian flow up to the timescale at which the wavepacket becomes so large that the Liouvillian dynamics ceases to be hyperbolic [37].

The uniformly hyperbolic Hamiltonian we consider is $\mathcal{H} = p_x^2/(2m) - m\lambda^2 x^2/2$. With the change of variable $p_x = (m\lambda/2)^{1/2}(q + p_q)$ and $x = (2m\lambda)^{-1/2}(q - p_q)/2$, the Hamiltonian can be written as

$$\mathcal{H} = \lambda\, p_q q - \mathrm{i}\hbar/2\ .$$

Solving the classical Hamilton equations of motion one gets $q(t) = q(0)\mathrm{e}^{\lambda t}$ and $p_q(t) = p_q(0)\mathrm{e}^{-\lambda t}$. Next, it is easily checked that a solution of the Schrödinger equation is provided by the wavepacket

$$\langle q|\psi(t)\rangle = A\exp[-\Delta^{-2}(t)[q - q(t) - \mathrm{i}\Delta^2(t)p_q(t)/\hbar]^2],$$

with $\Delta(t) = \Delta(0)\mathrm{e}^{\lambda t}$. Thus we see that a Gaussian wavepacket remains Gaussian, simply stretched and shifted by the Liouvillian flow. This quantum calculation is exact if the system is infinite. In finite systems, initially narrow classical distributions undergo a crossover from hyperbolic dynamics to diffusive behavior once their extension become comparable to some characteristic length scale of the system [1]. In our case we can thus expect that Gaussian wavepackets cease to be Gaussian once the wavepacket has spread to a width of order the lead width. In other words a Gaussian wavepacket will remain Gaussian for times shorter than the Ehrenfest time [37].

APPENDIX B: ALGORITHMIC CONSTRUCTION OF AN ORTHOGONAL PHASE-SPACE BASIS

A basis of coherent states can be made complete (and not overcomplete) but not orthogonal, by placing coherent states at the vertices of a von Neumann lattice [41]. This complete basis can be orthogonalized by following standard procedures (e.g. Gram-Schmidt orthogonalization), upon which, however, the basis states become very different from one another and extended in phase space. We here describe a numerical algorithm which orthogonalizes a complete basis of coherent states on a von Neumann lattice, while preserving the phase-space localization property of the basis states.

One starts from coherent states with wavefunctions

$$|\mathrm{cs}; i, j\rangle = \exp\big[-\tfrac{1}{2}|\alpha_{ij}|^2\big]\exp\big[\alpha_{ij}\hat{a}^\dagger\big]|0\rangle. \qquad \text{(B1)}$$

The creation and annihilation operators are (here $\hbar = 1$)

$$\hat{a}^\dagger = 2^{-1/2}[\hat{Q} - \mathrm{i}\hat{P}], \qquad \hat{a} = 2^{-1/2}[\hat{Q} + \mathrm{i}\hat{P}], \qquad \text{(B2)}$$

where $\alpha_{ij} = 2^{-1/2}[Q_i + \mathrm{i}P_j]$ and using dimensionless position Q and momentum P with $[\hat{P}, \hat{Q}] = \mathrm{i}$. The vacuum state, $|0\rangle$, is a Gaussian wavepacket centered at $P = Q = 0$,

$$\langle Q|0\rangle = \langle Q|\mathrm{cs}; 0, 0\rangle \ = \ \pi^{-1/4}\exp[-\tfrac{1}{2}Q^2]. \qquad \text{(B3)}$$

The coherent state (B1) is a Gaussian wavepacket centered at $Q = Q_i$ and $P = P_j$ with the same spread in both directions,

$$\begin{aligned}\langle Q|\mathrm{cs}; i, j\rangle \ &= \ \pi^{-1/4}\exp[\mathrm{i}P_jQ - \tfrac{1}{2}[Q - Q_i]^2],\\ \langle P|\mathrm{cs}; i, j\rangle \ &= \ \pi^{-1/4}\exp[-\mathrm{i}PQ_i - \tfrac{1}{2}[P - P_i]^2], \qquad \text{(B4)}\end{aligned}$$

where we have dropped irrelevant overall phases.

To get a complete basis, coherent states are placed at each vertex but one of a square von Neumann lattice, i.e. a regular lattice on the Q-P plane with each unit cell covering an area (2π) [41]. Translational invariance means that the empty lattice vertex may be anywhere. This basis of coherent states is complete but it is not orthogonal. To orthogonalize it, we make the ansatz that there exists a set $\{\beta_i\}$ such that the wavefunction

$$|\mathrm{ps}; i, j\rangle = \sum_{i',j'}\beta_{i'}\beta_{j'}|\mathrm{cs}; i' + i, j' + j\rangle \qquad \text{(B5)}$$

obeys

$$\langle \mathrm{ps}; k, l|\mathrm{ps}; i, j\rangle = \delta_{ik}\delta_{jl}\ . \qquad \text{(B6)}$$

Note that the form of Eq. (B5) is such that we assume that the basis-states will be symmetric under interchange of Q and P just as the coherent states are.

To satisfy Eq. (B6), we see that the elements of the set $\{\beta_i\}$ must obey

$$\delta_{i,0} \ = \ \sum_{i'i''}\beta^*_{i'}\beta_{i''}\ \exp[-(\pi/2)(i + i' - i'')^2] \qquad \text{(B7)}$$

Iterations	β_0	β_1	β_2	β_3	β_4	β_5	β_6	β_7	β_8	β_9	β_{10}
0	1	0	0	0	0	0	0	0	0	0	0
2	1.0386424	-0.1137192	1.93720E-2	-3.0781E-3	5.24E-6	4.3E-6	∼0	∼0	∼0	∼0	∼0
4	1.0357044	-0.1130793	1.74448E-2	-3.0142E-3	5.478E-4	-1.024E-4	1.95E-5	-3.8E-6	7E-7	-1E-7	∼0
6	1.0357044	-0.1130793	1.74448E-2	-3.0142E-3	5.478E-4	-1.024E-4	1.95E-5	-3.8E-6	7E-7	-1E-7	∼0
10	1.0357044	-0.1130793	1.74448E-2	-3.0142E-3	5.478E-4	-1.024E-4	1.95E-5	-3.8E-6	7E-7	-1E-7	∼0

TABLE I: Iterations of the orthogonalization algorithm for coherent states on a von Neumann grid. The table shows the value of $\beta_i = \beta_{-i}$ as the algorithm is iterated ($\beta_j \sim 0$ means that $|\beta_j| < 10^{-7}$). The algorithm converges with accuracy 10^{-7} after six iterations. Arbitrary large accuracies are obtained with more iterations. The PS-states are found by substituting the tabulated values into Eq. (B5).

We define a set of vectors, $\{v^{(\alpha)}\}$, written in a non-orthogonal basis, $\{\hat{e}_i\}$, such that $v^{(\alpha)} = \sum_i \tilde{\beta}_{i-\alpha}\hat{e}_i$, i.e. the ith element of the αth basis vector is $v_i^{(\alpha)} = \beta_{i-\alpha}$. The basis is chosen such that the basis-vectors have the inner product $(\hat{e}_i \cdot \hat{e}_j) = \exp[-(\pi/2)(i-j)^2]$. The condition that the vectors $\{v^{(\alpha)}\}$ form an orthonormal basis is

$$\delta_{\alpha,0} \;=\; (v^{(\alpha)} \cdot v^{(0)}) = \sum_{ij} \beta^*_{i-\alpha}\beta_j(\hat{e}_i \cdot \hat{e}_j) \qquad \text{(B8)}$$

This is identical to the condition (B7), thus orthogonalizing this set of vectors is equivalent to finding the β's which satisfy Eq. (B7). We use the following algorithm to orthogonalize these vectors

1. Take a complete normalized (but non-orthogonal) basis, $\{v_i\}$.
2. define a new basis such $\{v'_i\}$ such that $v'_i = A_i[v_i - \frac{1}{2}\sum_{j\neq i}(v_i \cdot v_j)v_j]$. We then choose A_i such that it normalizes the vector v'_i.
3. Repeat the procedure, taking the new basis $\{v'_i\}$ and deriving a basis $\{v''_i\}$, and so on.

We take the coherent states described above as the initial non-orthogonal basis, so initially $\beta_i = \delta_{i,0}$. In Table I we present data for the first ten iterations of the algorithm, by the sixth iteration the results satisfy Eq. (B7) with an accuracy of $\lesssim 10^{-7}$. Each iteration improves the accuracy by more than one order of magnitude. A PS-state generated by this procedure is shown in Fig. 6. We note that β_i decays approximately exponentially with i. Thus the PS-states given by Eq. (B5) are exponentially localized in position and momentum, as shown in Fig. 6.

Area-preserving stretches, $(Q, P, Q_j, P_j) \to (\kappa Q, \kappa^{-1}P, \kappa Q_j, \kappa^{-1}P_j)$, and rotations $(Q, P, Q_j, P_j) \to (Q\cos\theta + P\sin\theta, P\cos\theta - Q\sin\theta, Q_j\cos\theta + P_j\sin\theta, P_j\cos\theta - Q_j\sin\theta)$ are unitary operation for any κ, θ. Thus the stretched-rotated basis will also be orthonormal and complete. This legitimizes the procedure discussed in Section III B for optimizing the PS-basis by fitting it to the PS scattering band structure.

APPENDIX C: EDGE-OF-BAND PHASE-SPACE STATES

The tails of the PS-state shown in Fig. 6 decays exponentially with the number of lattice points away from the center of the PS-state. Strictly speaking, any PS-state has thus a finite amplitude outside the band. We can however treat PS-states as classical, i.e. completely inside one band, if they are more than $j_{\max}$ lattice sites away from the edge of that band. If we choose $j_{\max} = 1$, we would call states "classical" even if they have $\sim 3\%$ of their squared amplitudes outside the band (this is similar to the situation sketched in Fig. 7). If however we take $j_{\max} = 3$, then a PS-state is only classical if less than 10^{-5} of its squared amplitude is outside the band. The number of edge-of-band states (PS-states that are partially inside, partially outside a band with area $> 2\pi\hbar_{\rm eff}$) of a band which exits at time τ is

$$n_{\rm eob}^{{\rm L}\to K}(\tau) \simeq 4j_{\max}\left(\frac{W_{\rm L}W_K}{2\pi\hbar_{\rm eff}L^2}\right)^{1/2}\exp[-\lambda\tau/2], \quad \text{(C1)}$$

where $K = {\rm L}, {\rm R}$. Thus the number of edge-of-bands states is

$$N_{\rm eob} = \sum_K \int_0^{\tau_{\rm E}^{{\rm L}K}} {\rm d}\tau \mathcal{N}_{\rm band}^{{\rm L}\to K}(\tau) n_{\rm eob}^{{\rm L}\to K}(\tau) \;\sim\; \frac{j_{\max}N_{\rm qm}}{\lambda\tau_{\rm D}} \qquad \text{(C2)}$$

where the sum is over $K = {\rm L}, {\rm R}$ and $j_{\max}$ is a number of order one. Note that the error we make decays exponentially with $j_{\max}$, hence the choice of acceptable error only changes $N_{\rm eob}$ logarithmically. From Eq. (C2) we conclude that the edge-of-band PS-states are a subdominant proportion of the total number of quantum PS-states, and can be ignored.

[1] A.J. Lichtenberg and M.A. Lieberman, *Regular and Chaotic Dynamics*, (Springer-Verlag,New York,1992).

[2] J.-P. Eckmann and D. Ruelle, Rev. Mod. Phys. **57**, 617

(1985).
[3] L. Wirtz, J.-Z. Tang, and J. Burgdörfer, Phys. Rev. B **56**, 7589 (1997); this paper discusses the relevance of scattering bands to quantum transport in a regular billiard, but it does not make the connection between their area and the quantum phase-space resolution $\hbar_{\rm eff}$, nor does it discuss their occurrence in chaotic systems.
[4] P.G. Silvestrov, M.C. Goorden, and C.W.J. Beenakker, Phys. Rev. B **67**, 241301(R) (2003).
[5] J. Tworzydlo, A. Tajic, H. Schomerus and C.W.J. Beenakker, Phys. Rev. B **68**, 115313 (2003).
[6] J. Tworzydlo, A. Tajic and C.W.J. Beenakker, Phys. Rev. B **69**, 165318 (2004).
[7] Ph. Jacquod, and E.V. Sukhorukov, Phys. Rev Lett. **92** 116801 (2004).
[8] M.C. Goorden, Ph. Jacquod, and C.W.J. Beenakker, Phys. Rev. B (2005) **72**, 064526.
[9] The dwell time is exactly the same for all trajectories within a band for maps such as the kicked rotator used in Figs. 1 and 3.
[10] L.P. Kouwenhoven, C.M. Marcus, P.L. McEuen, S. Tarucha, R.M. Westervelt, and N.S. Wingreen, *Electron Transport in Quantum Dots*, Nato ASI conference proceedings, L.P. Kouwenhoven, G. Schön, and L.L. Sohn Eds. (Kluwer, Dordrecht, 1997); Y. Alhassid, Rev. Mod. Phys. **72**, 895 (2000); I.L. Aleiner, P.W. Brouwer, and L.I. Glazman, Phys. Rep. **358**, 309 (2002).
[11] H.U. Baranger, R.A. Jalabert, and A.D. Stone, Phys. Rev. Lett. **70**, 3876 (1993); H.U. Baranger, R.A. Jalabert, and A.D. Stone, Chaos **3**, 665 (1993).
[12] C.M. Marcus, R.M. Westervelt, P.F. Hopkings, and A.C. Gossard, Chaos **3**, 643 (1993).
[13] M. L. Mehta, *Random Matrices* (Academic, New York, 1991).
[14] R.A. Jalabert, J.-L. Pichard, and C.W.J. Beenakker, Europhys. Lett. **27**, 255 (1994); H.U. Baranger and P.A. Mello, Phys. Rev. Lett. **73**, 142 (1994).
[15] K.B. Efetov, Adv. Phys. **32**, 53 (1983).
[16] S. Müller, S. Heusler, P. Braun, F. Haake, and A. Altland, Phys. Rev. Lett. **93**, 014103 (2004).
[17] J. Müller and A. Altland, J. Phys. A **38**, 3097 (2005).
[18] G.P. Berman and G.M. Zaslavsky, Physica A **91**, 450 (1978).
[19] S. Oberholzer, E.V. Sukhorukov, and C. Schönenberger, Nature (London) **415**, 765 (2002).
[20] Ya.M. Blanter and M. Büttiker, Phys. Rep. **336**, 1 (2000).
[21] C.W.J. Beenakker and H. van Houten, Phys. Rev. B **43**, R12066 (1991); the semiclassical limit requires that one adapts the voltage in order to fix the injection rate of electrons, so $V \propto N_{\rm L}^{-1}$ as $\hbar_{\rm eff} \to 0$. If the voltage were fixed, the shot-noise power would diverge as $\hbar_{\rm eff} \to 0$. We thank Carlo Beenakker for a discussion of this point.
[22] O. Agam, I. Aleiner and A. Larkin, Phys. Rev. Lett. **85**, 3153 (2000).
[23] R.S. Whitney, and Ph. Jacquod, Phys. Rev. Lett. **94**, 116801 (2005).
[24] For a recent review on the quantum-to-classical correspondence in open systems see: H. Schomerus and Ph. Jacquod, cond-mat/0508092; to appear in J. Phys. A.
[25] I.L. Aleiner and A.I. Larkin, Phys. Rev. B **54**, 14423 (1996).
[26] İ. Adagideli, Phys. Rev. B **68**, 233308 (2003).
[27] J. Tworzydlo, A. Tajic and C.W.J. Beenakker, Phys. Rev. B **70**, 205324 (2004).
[28] S. Rahav and P.W. Brouwer, Phys. Rev. Lett. **95**, 056806 (2005); cond-mat/0507035.
[29] A semiclassical theory of transport at finite $\tau_{\rm E}$ can be made unitary once phase-space splitting is included in the theory, R.S. Whitney and Ph. Jacquod, in preparation.
[30] M.G. Vavilov and A.I. Larkin, Phys. Rev. B **67**, 115335 (2003).
[31] H.U. Baranger, D.P. DiVincenzo, R.A. Jalabert and A.D. Stone, Phys. Rev. B **44**, 10637 (1991).
[32] W. Bauer and G.F. Bertsch, Phys. Rev. Lett. **65**, 2213 (1990).
[33] H. Schomerus and J. Tworzydlo, Phys. Rev. Lett. **93**, 154102 (2004).
[34] I. Daubechie, *Ten Lectures on Wavelets* (SIAM, Philadelphia, 1992); G. Kaiser, *A Friendly Guide to Wavelets* (Birkhäuser, Boston, 1994).
[35] If the L lead is covered with PS-states placed on a square grid, then each PS-state has a spread of $\hbar_{\rm eff}^{1/2}$ in r and p. Thus a classical band which is narrower than $\hbar_{\rm eff}^{1/2}$ could not contain any PS-states, despite the band's phase-space area being $\sim \hbar_{\rm eff}^{1/2} W/L \gg \hbar_{\rm eff}$. This would lead to the prediction that the open cavity Ehrenfest time is $\lambda^{-1} \ln[\hbar_{\rm eff}^{1/2} W/L]$ (for $W_{\rm L} = W_{\rm R} = W$), which is half the value found by using the optimized PS-basis, see Eq. (8).
[36] In Eq. (11), λ is not strictly the Lypunov exponent, but rather the local rate of stretching of the Liouvillian flow averaged along the given trajectory. This distinction is important for the covering of non-parallelogram bands.
[37] E.J. Heller and S. Tomsovic, Phys. Today **46**(7), 38 (1993).
[38] P. Marconcini, M. Macucci, G. Iannaccone, B. Pellegrini, and G. Marola, cond-mat/0411691.
[39] F. Aigner, S. Rotter, and J. Burgdörfer, Phys. Rev. Lett. **94**, 216801 (2005).
[40] A. M. Chang, H. U. Baranger, L. N. Pfeiffer, and K. W. West, Phys. Rev. Lett. **73**, 2111 (1994)
[41] A. Perelomov, *Generalized Coherent States and Their Application*, (Springer-Verlag, Berlin, 1986).